Development of Notch Signaling Biomaterials as a tool to control stem cell behavior

Galante, JNR[1,2]

1- **NEWTHerapies Group, Biomaterials Division, INEB, University of Porto, R. Campo Alegre, 823, 4150-180 Porto (email: joao_ga1ante@hotmail.com)**
2- **Instituto Superior Técnico, 1049-001 Lisboa, Portugal**

***Abstract*— The Notch signaling pathway is a core regulator of cell-fate within several systems. The present work aims to create polymeric biomaterials with immobilized Notch ligands to activate Notch pathway, envisaging future clinical applications. As a platform, poly(2-hydroxyethyl methacrylate) (pHEMA) disks were synthesized and activated by N,N'-carbonyldiimidazole (CDI) at different concentrations (0; 0.03; 0.3; 3 and 30 mg/mL) and functionalized with an F(ab')$_2$ antihuman IgG-Fc specific fragment (Ab) in order to assure a correct exposure of the subsequently bound Notch ligand Delta-1-extIgG (Delta-1).The surfaces were characterized through FTIR-ATR and XPS. Moreover, the presence of Ab and Delta-1 was confirmed by FTIR-ATR, XPS and ELISA. The later also illustrated an accurate ligand orientation. The morphology was assessed by SEM, depicting a smooth surface unchanged after Ab immobilization. The biofunctionality of immobilized Delta-1 was evaluated using a T-cell lymphoblastic leukemia (T-ALL) cell line encoding the enhanced green fluorescent protein (EGFP) reporter gene (TALL-1-rbs-EGFP) and these materials were shown to trigger Notch signaling on TALL-1-rbs-EGFP cells. Immobilized Delta-1 with 0.3 mg/ml of CDI-activation was found to induce the highest Notch activation levels. Altogether, these results suggest a new biomaterial-based approach to control Notch signaling. For the first time, in a biocompatible polymeric substrate, different densities of immobilized notch ligand were shown to induce different signaling activation levels. More than representing and adequate apparatus for the study of Notch signaling pathway, these findings may portray a novel interface to control Notch mechanism in different cell systems, with an imminent leading role in HSC expansion.**

***Keywords*—** Notch; Biomaterials; pHEMA; Delta-1; Hematopoiesis; Surface functionalization.

I. INTRODUCTION

KNOWN as multipotent self-renewable cells capable of differentiating into all the mature blood cells that enter the circulation throughout life (hematopoiesis), Hematopoietic stem cells (HSC) are, along with hematopoietic progenitor cells, responsible for maintaining the number of circulating blood cells, that undergo continuous turnover [1]. When a disruption of any of the processes related to the tight regulation of the hematopoietic (stem) cells occurs, it can lead to a variety of blood malignancies. One is leukemia, amongst the most common forms of cancer in humans, characterized by uncontrolled growth and proliferation of abnormal blood cells (leukemic cells). Since conventional leukemia medical therapy (chemotherapy and/or radiotherapy) destroy both leukemia cells and the rapidly dividing blood-forming cells in the bone marrow (BM), the transplantation of HSC is imperative to replenish this organ with new blood cells [2]. Concerning transplantation, HSC are obtained either by BM aspiration, by peripheral blood after immobilization (PBSC), or by cord blood collection [3]. Traditionally, HSC from the BM have been used for stem cell transplantation [3]. However, a suitable family donor is found for less than 30% of patients who might benefit from this therapy, and the use of unrelated donors may not only call for several months before the unrelated donor is identified and the hematopoietic cells obtained but also encompass a higher risk of graft versus host disease (GVHD) [4]. As an extensively explored alternative within the last 20 years, UCB transplantation results in significantly lower rates of acute and chronic GVHD, possibly due the lower number and relatively naïve repertoire of the cord blood T cells [3-6]. Nonetheless, the amount of progenitor cells in each cord blood unit is ten times smaller than in BM or PB grafts, and it requires a high cell dose for optimum engraftment ($2.5x10^6$cells per kg patient body weight) which, given the diminutive volume of blood collected from a single UCB sample, limits the feasibility of direct transplantation of UCB for the treatment of pediatric patients [5-7]. Thus, augment HSC numbers is of foremost importance in the development of therapies for adult patients. Several ex-vivo culture systems have been designed, presenting variations concerning the use of a feeder layer, cytokine cocktail, culture media and static/dynamic culture conditions, in order to promote HSC expansion while controlling cell differentiation and envisaging the preservation of its engraftment ability [3,4,8,9]. However, the factors governing a return to G0/G1 (absolute prerequisite for long-term maintenance of HSC), the optimal combination and concentration of cytokines, as well as the more suitable ex-vivo culture conditions have not yet been determined [7,10].Therefore, alternative culture systems and conditions are being attempted. Amongst these novel approaches for HSC expansion is the use of Notch signaling ligand Delta-1 [5,11-13]. The Notch pathway is an evolutionally conserved signaling pathway, which has been related with a broad variety of processes, such as cell-fate determination, tissue patterning and morphogenesis, cell differentiation, proliferation and apoptosis, and a perturbation of it can manifest as tissue abnormalities and, in due course, lead to disease states such as certain forms of cancer (e.g. T-cell acute lymphoblastic leukemia - T-ALL, breast cancer, colorectal cancer, ovarian cancer, pancreatic cancer or lung carcinomas), cardiac disease or Alzheimer's disease [11,14-17].The mammalian family of Notch receptors consists of four members (Notch1–4) [16,18]. On the other hand, the Notch ligand family (so-called DSL family) consists, in mammals, of 5 type-I transmembrane proteins: Jagged1 and Jagged2, and

Delta-like 1, 3 and 4 (Dll1/3/4). When a Notch ligand comes in contact with Notch receptor, this interaction induces a conformational change in Notch receptors that lead to two successive proteolytic receptor cleavages which cause the Notch intracellular domain (NICD) to be released into the cytoplasm and be translocated to the nucleus causing the transcriptional activation of Notch target genes [16-19]. On the subject of hematopoiesis, Notch receptors are widely expressed throughout the hematopoietic system, from hematopoietic stem cells to more committed progenitors and hematopoietic tissues. Bernstein et al. demonstrated density-dependent effects of Delta1 on fate decisions, suggesting that the enhanced formation of B and T precursors occurs in the presence of lower densities of Delta1 and that higher densities of ligand lead mainly to T cell differentiation [20]. Furthermore, it was demonstrated that the induction of Notch signaling and subsequent fate of human $CD34^{+}CD38^{-}$ cord blood progenitors also depends on Notch ligand density [21]. Therefore, Notch-related data generated so far supports the concept that Notch signaling affects stem cell regulation by favoring self-renewal over differentiation, and that Notch ligands can increase HSC and maintain hematopoietic progenitor population in a quiescent and undifferentiated state, through a density-dependant action [10,22,23]. In addition, Notch pathway has been implicated in hematological diseases, including leukemias, lymphomas, and multiple myeloma [16]. Recently, activating mutations in Notch1 have been found in over 50% of human T-ALL, and overexpression of the Notch3 protein has been reported in virtually all cases of this hematological neoplasm [22,24] Taken as a whole, these observations demonstrate Notch signaling has a key context-specific regulatory role in hematopoiesis. Due to its influence on cellular fate, several strategies have been attempted in order to induce Notch signaling activation in vitro in the pursuit to understand and control this pathway and its manifold outcomes. The traditional approaches make use of: i) soluble forms of Notch ligands; ii) in vitro co-culture of Notch receptor-expressing cells with Notch ligand-presenting cells; iii) cell transfection encoding constitutively active forms of Notch Intracellular Domain (NICD); iv) ligands immobilization onto standard tissue-culture polystyrene (TCPS) plates; or v) more recently, the development of biomaterials with immobilized Notch ligands [13,17,24-29].Although some preliminary results were obtained, the use of soluble ligands (ligand extracellular domain) is believed to be unlikely to activate Notch signaling, typically by demonstrating no activity or even antagonistic properties unless clustered by an antibody [26,30]. Regarding the co-culture strategy, the miscellany of cell-to-cell interactions hinders an isolated study of Notch mechanism, and the possibility of some heterogeneity among the cell lines and cell culture conditions may possibly give rise to variations on ligands expression levels [17]. Therefore, ligand immobilization strategies have been extensively described on literature. Traditional approaches consisted of ligand coatings on TCPS plates. In particular, an engineered form of Delta-1 (Delta-1-extIgG) has been reported as being essential for Notch activation, and this strategy is already in Phase I clinical trials for cord blood expansion and confirmed as capable of rapid myeloid reconstitution [25]. Notwithstanding these results, the immobilization onto TCPS can hold several setbacks. This system does not afford protein specificity, does not provide reproducible physical properties (e.g., conductivity, wettability) and does not assure the control of ligands orientation due to plastic brand variations or sterilization procedures [17,28,29]. To overcome these limitations, biomaterial-based strategies came into sight. SAMs are model surfaces structured at the nanoscale that can be modified in order to expose specific functional groups or proteins (functionalization), and have been used to screen diverse biological processes such as platelets adhesion and activation, immobilized epidermal growth factor (EGF) bioactivity, leukocytes adhesion or mesenchymal stem cells differentiation [28,31,32]. In particular, the utilization of SAMs to indirectly (i.e. through an intermediate antibody, in order to bind the Fc-engineered ligand by its Fc fragment tale) immobilize Jagged-1/Fc chimeric protein has proven to be able to monitor ligand orientation which, together with density control, can be used to induce different signaling levels [17]. However, SAM' structure is susceptible of oxidation, which will disrupt the assembled monolayer, thus turning crucial to transpose this knowledge to real world polymers. On the first polymer-based approaches to immobilize Notch ligands, the use of streptavidin-coated superparamagnetic polystyrene microbeads had a drawback that consists on the microbeads tendency to aggregate, providing nonuniform signaling to the cells [29,33]. As an alternative, polymeric hydrogels, broadly used for biomedical/pharmaceutical applications such as controlled drug release and delivery, wound management and tissue engineering due to its biocompatibility, good transport properties, injectability, and to its ease of construction and potential to be chemically, physically and mechanically modified, have emerged [34,35]. Innovatively, 3D polyacrylamide hydrogel inverted colloidal crystal (ICC) scaffolds (highly organized and uniformly-sized spherical pores well interconnected with adjacent pores) have been coated with Delta-1 notch ligand through a layer-by-layer (LBL) molecular assembly technique [13]. This approach demonstrated to be capable of preserving ligand bioactivity and promote pre-T-Cell differentiation of HSC. Nonetheless, therein the ligand was directly coated onto the LBL modified scaffolds, which does not guarantee a proper and controlled ligand orientation. In addition, it was denoted a strong cellular association with the LBL-coated surface, which may hinder possible applications into the HSC expansion field (difficult cell harvesting). Hence, low-fowling polymeric strategies came out. Belonging to the polymer family of methacrylates, poly(2-hydroxyethyl methacrylate) (pHEMA) is a synthetic nontoxic hydrogel which can be easily polymerized and presents low fowling (low protein adsorption and cell adhesion) properties, being widely exercised in biomedical area [36-39]. Well known for its use

in soft contact lens, pHEMA has been extremely useful for other biomedical applications such as catheters, intrauterine inserts, artificial skin, or as a basis for drug delivery [38]. Concerning Notch ligands immobilization, pHEMA has been exploited by Beckstead et al that, comparing direct and indirect immobilization schemes, shown that Jagged-1 indirectly (i.e. by affinity, through a previously immobilized antibody) bound to the pHEMA surface results in greater potency to induce Notch signaling and differentiation in human derived Keratinocytes, demonstrating the importance of ligand orientation [27]. Therefore, effective strategies to control and monitor ligand concentration on alternative substrates, as pHEMA, could overcome the limitations of the current systems and bring new insights on therapeutic potential of Notch signaling pathway. The final scope of this work is to immobilize different densities of human Notch ligands in polymeric substrates in order to induce and control Notch signaling activation. Based on work recently performed on model SAMs, a chimeric form of Notch ligand Delta-1 engineered with an Fc fragment of a human immunoglobulin (Delta-1-extIgG) will be indirectly immobilized to the surface of pHEMA [17]. Using a T-ALL cell line as a model, it is expected that different levels of Notch signaling activations would be attained.

II. MATERIALS AND METHODS

II.1. PREPARATION OF PHEMA CROSS-LINKED FILMS

Cross-linked pHEMA films were synthesized from 2-Hydroxyethyl methacrylate (HEMA, Polysciences, cat. 04675) monomer with a purity of more than 99.5%, as previously described [43]. In brief, 5 ml of HEMA and 0.23 ml of tetraethylene glycol dimethacrylate (TEGDMA; Polysciences, cat. 02654) cross-linking agent were added to a water/ethylene glycol (J.T.Baker, cat. 7037) mixed solvent (1 ml/1.5 ml) with 1 ml of each of the two redox initiators, 40% ammonium persulfate (APS; 98%, Aldrich, cat. 24,861-4) and 15% sodium metabisulfite (SMB; 97%, Aldrich, cat. 25.555-6), towards setting in motion the radical polymerization. The mixture was allowed to polymerize, overnight, between two clean glass plates with a Teflon gasket of thickness 0.25 mm, even though the gel sets within an hour (it resided overnight to assure that the polymerization flawlessly occurred). In the day after, pHEMA film was released from the glass plates and soaked in distilled water for 4 h (water renovated every hour) to leach out unreacted monomers, initiators, and oligomer residues since, although some reports point toward a longer leeching process, most the impurities are known to be washed out within the first few hours. After leaching, the pHEMA film was cut with a punch into 8 mm diameter discs, which were vacuum-dried between two Teflon sheets and glass plates so as to flatten the surface, and because water molecules can disable the linkage between the hydroxyl group on the pHEMA surface with the carbonyl group of N,N'-carbonyldiimidazole (CDI). Subsequently, the samples were maintained in argon until the next step.

II.2. ACTIVATION OF THE OH GROUPS OF PHEMA

Prior to activation/immobilization procedure (24h), the flasks, pipettes, spatula and forceps required were rinsed 3 times with tetrahydrofuran anhydrous (THF; 99.9%; Aldrich, cat.18.656-2) under 5 minutes of ultrasounds and dried overnight at 80ºC, together with the scintillation vials used in the immobilization, to eliminate any trace of humidity. Under a dry nitrogen atmosphere, pHEMA disks were immersed in CDI solutions (N,N'-carbonyldiimidazole, SIGMA, cat. 21860) with the following concentrations: 0; 0.03; 0.3; 3 and 30 mg/mL, in diverse solvents. The solvents tested include: N,N-dimethylformamide anhydrous (DMF; 99.9%, Aldrich, 27,705-6), Dry Acetone (Merck, cat. 1.00299) and anhydrous THF. The activation occurred during 2h at 45ºC under high-speed shaking (315 rpm). After reaction, activated pHEMA disks were washed, three times with the respective solvent, under 5 minutes with ultrasounds (to remove unreacted CDI).

II.3. IMMOBILIZATION OF ANTIBODY (AB) IN PHEMA

Two different antibodies were used. For the reaction optimization, a regular human IgG (Zymed cat. 02-7102) was utilized (10 and 100 µg/mL). For our purpose, an affinipure $F(ab')_2$ antihuman IgG-Fc specific fragment (Jackson Immunoresearch, cat 75848**)** was used (10 µg/mL).Towards the optimization of immobilization reaction, two different pHs were attempted: pH=7.4 and pH=9.15 [17,31]. CDI-activated pHEMA disks were immersed in Ab solutions prepared in sterile Phosphate Buffer Solution (PBS, pH 7.4, Sigma) or in sterile Sodium Borate solution (Borax, 0.01M, pH 9.15). Appropriate controls were prepared without Ab. All the samples were maintained under Argon environment, during 24h at 4ºC, in swift stirring (420 rpm). After 24 hours, disks were removed to new scintillation vials and rinsed three times (5 minutes, 420 rpm) with PBS or Borax (pH 7.4 and pH 9.15, respectively).

II.3.1 SURFACE CHARACTERIZATION

To characterize CDI activation and Ab immobilization steps, different surface characterization techniques were tested: Fourier transform infrared spectroscopy with attenuated total reflectance (FTIR-ATR), X-ray photoelectron spectroscopy (XPS), scanning electron microscopy (SEM), Bicinchoninic acid (BCA) assay and enzyme-linked immunosorbent assay (ELISA).

II.3.1.1. FTIR-ATR

All spectra were obtained on a Perkin Elmer FTIR spectrophotometer model 2000, coupled with an ATR accessory (SplitPeaTM from Harrick Scientific) provided with a silicon internal reflection crystal, at external reflectance mode. Before analysis, all disks was carefully dried under vacuum, in order to lower the influence of water absorbance on polymer spectra, and carefully cleaned. After placing the disks on the ATR accessory, a 2.5Kg heaviness, homogeneously applied on a fixed area of the disks with the ATR accessory pressure plate, was found to give a good air-free contact between the samples and the crystal. Hence, all data were taken at 2 cm^{-1} resolution with a total of 100 scans, and measurements were performed in the mid-IR frequency range (4000–600 cm^{-1}). Using the Spectrum® (PerkinElmer Inc., version 5.3.1) software, the ATR spectra were obtained by taking the ratio of each sample spectrum with the corresponding "free-standing" background spectrum, thus improving, together with subsequent baseline correction and smoothening, spectrum quality.

II.3.1.2. XPS

X-ray photoelectron spectroscopy (XPS) was used to study the chemical composition of pHEMA and modified pHEMA surfaces. Vacuum-dried disks were analyzed on a VG Scientific ESCALAB 200A (UK) spectrometer, using magnesium $K\alpha_{1,2}$ (1253.6 eV) as radiation source to stimulate photoemission. At room temperature, the emitted photoelectrons were analyzed at a takeoff angle of 90º (i.e. with an angle of 90º between the surface of the sample and the detecting crystal), providing information of about 100 Å of the uppermost surface of the sample. Survey spectra were collected, over a binding energy (BE) range of 0-1100 eV, with analyzer pass energy of 50 eV (a relatively high pass energy thus permitting rapid data acquisition and accurate quantitative analysis, being useful to determine each surface elemental composition) [40]. High resolution C(1s), O(1s) and N(1s) scans were obtained with a pass energy set at 20 eV (lower pass energies provide higher energy resolution). Subsequently, a XPS fitting program (XPSPEAK, version 4.1) was used to resolve the high resolution spectra into individual Gaussian peaks, and calculate these integrated peak areas. The maximum of the resolved C(1s) spectrum, which corresponds to the peak of carbon in hydrocarbon environment

(CH_x),was set to 285.0 eV. In order to adjust the binding energy scales of each element. Furthermore, this setting not only served as reference for adventitious carbon contamination but also took into account possible shifts caused by charging of the sample surface [41]. As well, atomic concentrations were quantified using the integrated peak areas and tabulated sensitivity factors.

II.3.1.3. SEM

Surface topography of modified pHEMA was acquired with a scanning electron microscope (SEM). To prevent the accumulation of static electric charge on the surface throughout electron irradiation, all the previously vacuum-dried disks were coated with graphite of 20 nm thicknesses becoming electrically conductive. Graphite coating is regularly used on polymers (as non-metallic samples). Gold coating, as previously used on SAMs, can overheat the samples creating surface features which, more than damaging the sample, may be misleading when interpreting results and thereby were not used. Then, the surface of all pHEMA, activated pHEMA and Ab-pHEMA samples was observed, with 200x and 500x magnifications, in a FEI QUANTA 400 FEG environmental scanning electron microscope coupled with an EDAX PEGASUS X4M. The later allowed the elemental composition of specific zones of the samples to be determined by energy dispersive spectrometry (EDS). During observations, it was used an accelerating voltage of 15eV.

II.3.1.4 BICINCHONINIC ACID (BCA) PROTEIN ASSAY

To detect the presence of immobilized Ab on pHEMA disks, BCA microplate assay was performed using BCA protein assay kit (Pierce, cat. 23225), according to the manufacturer instructions 94. Briefly, three Ab-pHEMA replicates, and respective Ab-free controls, for each CDI concentration were placed onto a 48 well-polystyrene cell culture plate. The BCA working reagent (WR) was prepared by mixing 50 parts of BCA Reagent A (containing sodium carbonate (Na2CO3), sodium bicarbonate (NaHCO3), bicinchoninic acid ((HO2CC9H5N)2) and sodium tartrate (Na2C4H4O6) in 0.1 M NaOH) with 1 part of BCA Reagent B (containing 4% cupric sulfate, CuSO4·5H2O) (50:1, Reagent A:B). Then, the disks were incubated with 200 µL of WR at 37ºC for 30 minutes, after which the plate was taken to reach RT again, and the supernatants were transferred to a 96 well plate and the absorbance was read at 562 nm on a Biotek PowerWave XS plate reader.

II.3.1.5. ENZYME-LINKED IMMUNOSORBENT ASSAY (ELISA)

To detect Ab immobilization onto pHEMA activated disks, an ELISA was designed using an Anti-Rabbit IgG antibody, peroxidase-conjugated (Sigma cat. A0545, 0.01M) to detect Ab (raised in rabbit). Once more, three replicates of Ab-pHEMA disks at each CDI concentration and respective controls were investigated. Ab adsorption in polystyrene wells was used as a positive control (150 µL of Ab solution (10 µg/mL) were adsorbed during 30 min at 37ºC). To perform this ELISA, 48-well plate was previously blocked with 150 µL of a blocking solution containing 3% of bovine serum albumin (BSA) in phosphate buffered saline (PBS) (with an exception to Ab-TCPS wells) for 1h at 37ºC to prevent non-specific binding of peroxidase-conjugated antibody. The disks were, then, inserted onto the previously blocked wells with the anti-rabbit IgG-peroxidase antibody (1:4000 dilution in PBS-BSA 3%) for 1h at RT. After that, samples were rinsed with PBS/Tween 20 (0.05%) solution. The substrate solution was prepared freshly using o-phenylenediamine dihydrochloryde (Sigma, cat. P1526, 1 mg/mL) in phosphate citrate buffer 0.05M (Merck, cat.109885, pH=5.0), with 0.03% H2O2 (Merck, H2O2 30%, cat.1.12018), and Ab-pHEMA discs were incubated with 150µL of substrate solution during 10min at RT. The reaction was stopped with 150 µL of 1M H2SO4. 200 µL of the resulting solution were transferred to a new 96-well plate and absorbance was read at 450/630 nm dual wavelength (630 nm absorbance was subtracted to eliminate plate artifacts) using a Biotek PowerWave XS plate reader.

II.4. BINDING OF DELTA-1-EXTIGG LIGAND TO AB-PHEMA DISKS

After the immobilization of Ab on pHEMA discs, these were placed in a 48-well plate and incubated with Delta-1-extIgG (150uL, 10ug/ml) during 2h at 37ºC. Delta-1-extIgG produced at Fred Hutchinson Cancer Research Center (FHCRC) was kindly gifted by Irwin D. Bernstein. Note that for XPS analysis, Delta-1 was directly added to Ab-pHEMA, while for ELISA and posterior cell studies, Ab-pHEMA was previously blocked with PBS-BSA3% 1h at 37ºC, before Delta-1-extIgG incubation to its prevent non-specific binding.

II.4.1. SURFACE CHARACTERIZATION

To assess the binding and orientation of Delta-1-extIgG onto Ab-pHEMA disks, surface characterization was performed by XPS and ELISA assays.

II.4.1.1. XPS

To characterize Delta-1-extIgG binding to Ab-pHEMA discs, XPS spectra was obtained as described for Ab-pHEMA and the N percentage related with the amount of bound protein.

II.4.1.2. ELISA

ELISA assay was used to detect the presence of Delta-1-extIgG on Ab-pHEMA disks using two different antibodies: a monoclonal anti-human DLL-1 antibody (RnDsystems, MAB18181) (anti-DLL-1) and a monoclonal anti-human IgG1, Fc fragment (Millipore, CBL309) (Anti-Fc). Anti-Dll-1 was used to detect the extracellular domain of Delta-1 and Anti-Fc was used to detect the presence of Fc fragments. Adsorbed Delta-1-extIgG in polystyrene (with and without previously adsorbed Ab) were used as ELISA controls. As formerly described, the 48-well plate was previously blocked with PBS-BSA 3%, for 1h at 37ºC. Delta-1-extIgG-Ab-pHEMA disks (3 to 5 replicates per condition) were then incubated with 150ul of anti-Dll1 (1:1000) or with anti-Fc (1:1000) during 1h at RT. After that samples were rinsed with PBS/Tween 20 (0.05%) and incubated with a goat anti-mouse affinipure $F(ab')_2$ fragment IgG (dil 1:1000, Jackson ImmunoResearch, cat. 115-036-006) peroxidase-conjugated (secondary antibody**).** After rinsing with PBS/Tween 20 0.05%, 150 ul of substrate solution was added (o-phenylenediamine dihydrochloryde solution (1 mg/ml) in phosphate citrate buffer 0.05M (pH=5.0) with 0.03% H_2O_2). The samples were incubated during 10min at RT and the reaction was stopped with 150ul of H_2SO_4 1M. 200 µL of the resulting solution were transferred to a 96-well plate, and absorbance was measured (Dual wavelength) using a Biotek PowerWave XS plate reader.

II.5. ACTIVATION OF NOTCH RECEPTOR BY DELTA-1-EXTIGG-AB-PHEMA SURFACES

II.5.1. T-ALL-1-RBS-EGFP CELL CULTURE

As a cellular model for Notch receptor activation, human T-lymphoblastic cell line previously transduced with a lentiviral vector encoding the enhanced green fluorescent protein (EGFP) reporter was used. T-ALL-1-rbs-EGFP cells were gently provided by Dr. Stefano Indraccolo (Istituto Oncologico Veneto-IRCCS, Padua, Italy). This suspension cell line was maintained in RPMI-1640 medium with L-Glutamine (cat. 21875, Gibco) supplemented with 10% of fetal bovine serum (FBS) (Gibco), 1% of sodium pyruvate (NaP) and Penicilin:Streptomycin (P/S) antibiotics at 37ºC, fully humidified atmosphere with 5% CO_2 [95]. The cells were allowed to grow and at 70-80% of confluence (i.e. in the log phase of growth), every 3-4 days, cells were counted and divided (from $2x10^5$ cells/ml up to $10x10^6$ cells/ml) Cell counting and assessment of viability were performed by trypan blue dye exclusion method. Briefly, 10µL of cell suspension were mixed with 10µL of 0.4% trypan blue**,** and 10µL of the mixture were transferred to a Neubauer chamber (or haemocytometer) where viable **(**white**)** and dead **(**blue**)** cells were discriminated under an optical microscope (Olympus CK 2).

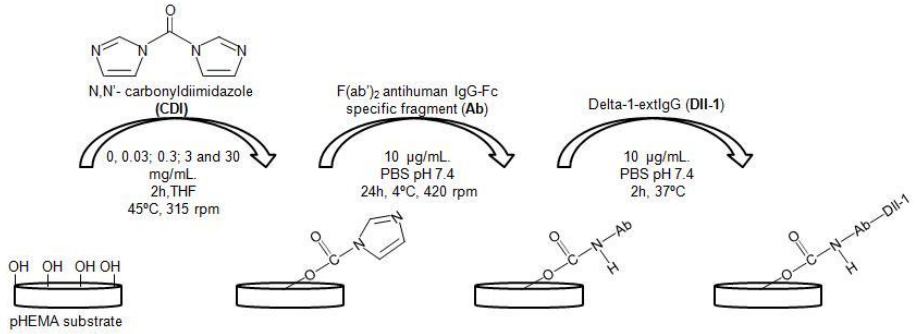

Figure 1- Experimental design of Notch ligand immobilization reaction. pHEMA disks were activated with CDI of 0, 0.03, 0.3, 3 and 30 mg/mL. Subsequently, F(ab') $_2$ antihuman IgG-Fc specific fragment (Ab) was immobilized at 10 µg/mL, at pH 7.4. Finally, A chimeric form of Delta-1, engineered with an Fc fragment of a human immunoglobulin was bound to the immobilized Ab at concentration of 10µg/mL.

II.5.2. ACTIVATION OF NOTCH RECEPTOR ON T-ALL-1-RBS-EGFP CELL LINE

TALL-1-rbs-EGFP cells were incubated with Delta-1-extIgG-Ab-pHEMA, and activation of Notch receptor was assessed by EGFP expression by flow cytometry. The protocol was firstly optimized in terms of incubation time with the cells and cell concentration using adsorbed ligands to polystyrene plates.

II.5.2.1. TIME OPTIMIZATION AND CELL CONCENTRATION OPTIMIZATION

Cell concentration, per ligand, and activation time period influence Notch receptor activation. 2x10^5 cells/ml were cultured in a 24-well plate during, 72 and 96h in the presence of previously adsorbed proteins: Delta-1 (10 ug/ml), Jagged-1 (RndD, cat. 599-JG, 10 µg/mL). Adsorbed human IgG (Zymed, cat. 02-7102, 10 ug/ml) and TCPS were used as negative controls. The proteins were adsorbed overnight at 4ºC. At the time points referred, cells were harvested and EGFP expression assessed by flow cytometry. To optimize cell concentration for receptor activation, 1x10^5 and 2x10^5 cells /ml were seeded on Jagged-1 coated wells as described before. EGFP expression was assessed past 96h.

II.5.3. CULTURE OF T-ALL-1-RBS-EGFP CELLS ON DELTA-1-EXTIGG-AB-PHEMA

2x10^5 cells/ml were incubated during 96h in a 48-well plate with Delta-1-ext-IgG-Ab-pHEMA disks prepared with different CDI concentration: 0; 0.03; 0.3; 3 and 30 mg/ml (3 replicates/each), as described in II.III. As controls, Delta-1-extIgG was adsorbed on TCPS with and without previously adsorbed Ab (10 µg/mL). After 96h, cells were harvested and EGFP expression assessed by flow cytometry.

II.5.3.1. EGFP EXPRESSION ANALYSIS BY FLOW CYTOMETRY

After culture, TALL-1.rbs-EGFP cells were harvested, centrifuged 5min at 1200 rpm on a microcentrifuge (Eppendorf, 5417 R) to remove cell debris, and the cell pellet was re-suspended in 200µL of 1% (w/v) Paraformaldehyde (PFA, Sigma). Cells (10000 events) were run on a FACScalibur (BDBiosciences) and EGFP expression assessed using the CellQuest software (BD). The Median Fluorescence Intensity of each cell sample was determined using FLOWJO and, when necessary, corrected per area of immobilized ligand.

III. RESULTS AND DISCUSSION

III.1. Material preparation

III.1.1. pHEMA

Analyzing the pHEMA IR spectra (Figure 2), it is possible to identify the characteristic PHEMA absorption bands. Starting from high-frequency region, the first wide band (~3424 cm^{-1}) is known to be assigned to the hydroxyl groups (-OH) stretching vibrations, and the bands occurring between 2800 and 3050 cm-1 are linked to the symmetric and antisymmetric C-H stretching vibrations of CH_2 and CH_3 groups within the polymer [44]. Approximately at 1720 cm^{-1}, another characteristic pHEMA absorption band takes place, linked to the ester stretching band of the carboxyl group (C=O) [43]. At 1158 cm^{-1} and at 1077 cm^{-1}, the bands correspond respectively to the stretching band of the alcohol group (C–O) and to the absorption bands typical of the carboxylic acid esters [40]. Also important to highlight is the 1458 cm^{-1} band, corresponding to asymmetric methyl bending (CH_3). In addition, the band at 1636 cm^{-1}, distinctive of the stretching vibration of the C=C double bond, is not detected within the analysis demonstrating that all the monomer has been polymerized. It is also possible to confirm the absence of water in pHEMA spectra. This aspect, particularly important for the subsequent steps of

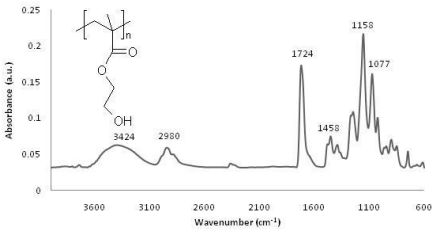

Figure 2- IR absorbance spectra of pHEMA

chemical modification, can be wrapped up from the spectrum. Therein, the ~2130 cm^{-1} band, only observed in wet samples and derived from a combination band of the H-O-H bending vibrations (~1650 cm^{-1}) and the librations (~700 cm^{-1}) of bulk water molecules is not found [12]. Moreover, the firstly described OH stretching vibration band is known to be shifted to lower frequencies (~3380 cm^{-1}) when water is within the sample, and the absorption is strongly augmented when in comparison to the obtained. From the preliminary survey XPS spectra of

pHEMA, it was possible to identify diverse elements on the films surface, although only carbon (C) and oxygen (O) were expected. However, these contaminants were partially removed on subsequent experiments through a more efficient wash of the glasses and Teflon sheets (data not shown).

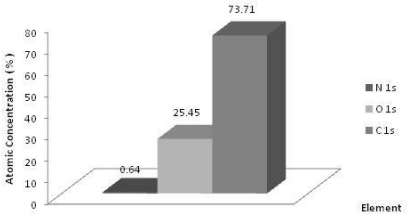

Figure 3- Atomic concentrations of the pHEMA elements, provided by XPS.

Moreover, and despite finding a minute percentage of Nitrogen, the atomic composition found for the surface of pHEMA (Figure 3) was close to the theoretical values for this polymer (66.7% of carbon and 33.3% of oxygen), with a C/O ratio of 2.9 [40]. In accordance with Gonçalves et al., the C(1s) high-resolution XPS spectrum of pHEMA (Figure 4) consists of three main peaks: a CH_x peak at 285.103 eV, respecting to carbon with no bounds to Oxygen (hydrocarbons); a C-O peak at 286.735 eV, and an O-C=O peak at 289.011 eV [36], observed after spectral resolution into individual Gaussian peaks.

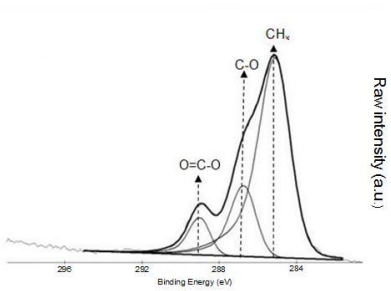

FIGURE 4- Typical XPS high resolution C(1s) spectra of pHEMA. From left to right, peaks corresponding to O=C-O, C-O and C-H_x bounds can be observed.

Even though it emerges at the correct region, CH_x peak appears more intense than it is typically seen for pHEMA [43]. Being issued to hydrocarbons, this peak height is highly sensitive to the presence of organic contaminants that can easily be deposited within the experimental procedure on the lab [43,45]. Together, these evidences indicate that the analyzed material was, indeed, pHEMA, which was geared up (after the depicted contaminant prevention procedures) for the subsequent steps of the experimental work.

III.1.2. CDI ACTIVATION

Following the synthesis of pHEMA, it is necessary to activate the hydroxyl groups of pHEMA to allow a covalent bound between the polymer and a protein. Therefore, N,N'-carbonyldiimidazole (CDI), was exploited, due to its ability to react with alcohol, carboxylic acid and amine groups giving rise to reactive carbonyl imidazole intermediates that can subsequently undergo selective reactions with primary amines or primary alcohols [36]. Hydroxyl groups on the surface of the produced low-fouling polymer can, thus, be activated via generating a carbamate linkage between the surface and one of the CDI molecule's imidazole (Figure 1) [31]. The hydroxyl groups' activation with CDI was already optimized, within model surfaces, in previous works from the group [17,28,31,32].Nevertheless, and although pHEMA activation with CDI has been performed once, a concentration gradient of this activator was never attempted for this purpose [27]. This gradient aims to, by reaching a range of quantities of immobilized antibody, obtain different Notch ligand densities and, therefore, achieve and monitor possible variations on Notch signaling activation levels. A range of CDI concentrations was primarily used instead of different protein concentrations to allow the reduction of non-specific protein binding, as previously demonstrated [31]. Subsequent to solvent selection, wherein anhydrous Tetrahydrofuran (THF) was elected as the most suitable one, and to the optimization of washing procedure, where the use of ultrasounds has shown to more efficiently remove unreacted CDI, the activation process was evaluated (Figure 5).

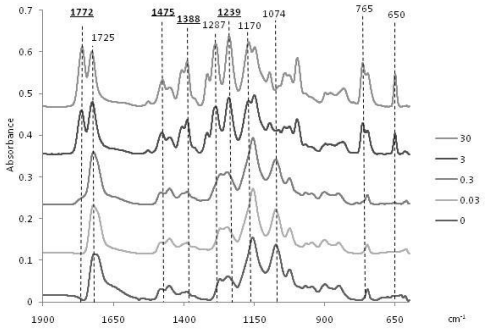

Figure 5- IR absorbance spectra of pHEMA disks activated with different CDI concentrations: 0; 0.03; 0.3; 3 and 30 mg/mL. The CDI characteristic peaks are discriminated in bold.

Therefore, five different degrees of activation were scrutinized (CDI concentrations equal to 0; 0.03; 0.3; 3 and 30 mg/mL). In accordance to Hye Jin Lee et al, four CDI characteristic infrared absorption bands, respecting the imidazolyl-carbamate groups, appeared in the absorbance spectra [45,46].

The asymmetric stretch of the CDI carbonyls derives the 1772 cm^{-1} band, at 1475 cm^{-1} the imidazole inner deformations are detected, and the C-N stretches give birth to the 1388 cm^{-1} and 1239 cm^{-1} bands. It is also possible to verify that the ester stretching band of the pHEMA carboxyl group is maintained at 1722 cm^{-1} in addition to the 1170 cm^{-1}, also pHEMA characteristic and matched to the C–O stretching. Notwithstanding the

maintenance of the referred bands, at 1074 cm^{-1} the typical carboxylic acid esters absorption band gradually disappears while the CDI concentration grows. In addition, the 765 cm^{-1} and 650 cm^{-1} may derive from functional groups possibly created amid the imidazolyl-carbamate groups and unreacted CDI molecules [47]. The maintenance of some of the pHEMA bands while others disappear may indicate that the CDI possibly did not react among the entire polymer surface. Nevertheless, the CDI activation step has been confirmed and the material was ready for the immobilization step.

III.1.3. ANTIBODY IMMOBILIZATION

After activation of pHEMA substrates, it is time for the antibody immobilization to take place. Hence, on the CDI-activated hydroxyl groups, the primary amine group of the antibody (N-nucleophile) attacks the electron-deficient carbonyl, displacing the nontoxic imidazole and coupling the protein to the activated pHEMA (Figure 1) [48-50].Towards the immobilization optimization, two pH conditions were tested to covalently immobilize an antibody. It was already demonstrated in the literature that pH 9 is the more effective pH that favors the substitution of the imidazole group for a protein [27,31,36]. However, it is also demonstrated that this immobilization reaction can be performed at pH 7.4, which guarantees the maintenance of the protein structure, an aspect particularly important for the antibody recognition sequences [17,28]. To optimize the immobilization reaction, only two CDI concentrations were used (0 and 3 mg/ml) and a non-specific human immunoglobulin (IgG) (bigger than the $F(ab')_2$ fragment, thus easily screened) was used.

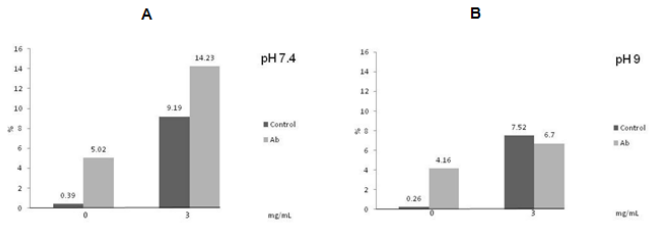

Figure 6- Nitrogen percentage detected by X-ray photoelectron spectroscopy in relation to IgG (10 µg/mL) immobilization on CDI-activated pHEMA disks, with [CDI]=0 and 3 mg/mL. pH =7.4 (A) and 9 (B). The series refer to presence (Ab) and absence (Control) of the antibody - IgG.

Not requiring specific sample preparation, FTIR-ATR was performed since the modifications resulting from antibody immobilization are expected to occur at the very surface of the polymeric disks [27]. However, no noteworthy differences between the two pHs were detected (data not shown). One hypothesis may be the fact that, given that FTIR-ATR beam can go 5 µm deep in the material, although the immobilization reaction may be occurring the protein signal is masked within the polymer spectra. In accordance, the low protein concentration (10 µg/mL) might also be negatively affecting the accuracy of the results brought by this surface characterization method. Therefore a more superficial technique was needed. Hence, XPS method was the ensuing tool utilized. Since the pHEMA background does not present nitrogen (N) on its structure, N spectrum was used to monitor the amount of protein immobilized at both pHs (Figure 6). Concerning the disks not activated by CDI with adsorbed protein, although the nitrogen percentages are similar in both pH's, a slightly higher percentage is noticed at pH=7.4 (5.02%, facing the 4.16% that come into sight at pH=9). This fact may be indicative that the protein adsorption (non-covalently bound) was weakened at pH=9. Also at pH 9, a slightly lower percentage of N can be observed in the CDI-activated protein-free disks comparatively to its counterpart at pH 7.4. This difference can point to a possibly more effective removal, at pH 9, of residual CDI that was still remaining after the washing step. Concerning the CDI-activated disks with immobilized protein ([CDI]=3mg/mL), sizeable differences come out among the two pH conditions. At pH=7.4 the nitrogen percentage (14.23%) is more than twofold increased face to the obtained at pH=9 (6.7%). The adsorption does not significantly differ among the two pHs and, despite having been used by other groups, pH 9 may cause alterations in the biological activity and protein integrity (tertiary and quaternary structure, disulfide bridges and hydrogen bonds) [17,27,36].

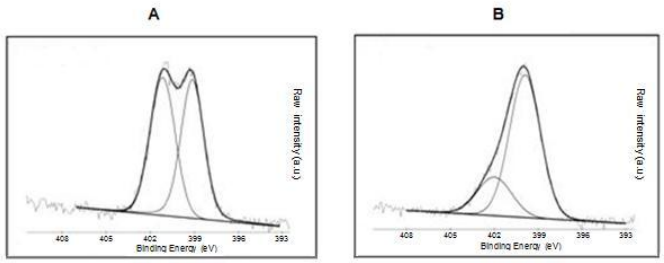

Figure 7- Typical XPS high resolution N(1s) spectra of CDI-activated pHEMA with (B) and without (A) immobilized IgG at 10µg/mL. [CDI]=3mg/mL.

Therefore, and in agreement what was previously performed by our group for Jagged-1 immobilization on SAMs, it was opted for pH 7.4 for the immobilization reaction [17]. Furthermore, since it was observed that CDI is not completely removed during the washing procedures before protein immobilization, the XPS N (1s) was analyzed in more detail. Although pHEMA does not contain N on its structure, both CDI imidazole group and peptide possess N [27,36]. But despite the presence of Nitrogen in both the imidazole rings and the peptide, the correspondent XPS Nitrogen (1s) peaks are described as being dissimilar. Throughout the analysis of Figure 7 A, an imidazole-derived doublet with maxima at 399.1 and 401.2 eV is depicted. This confirms the successful activation of the pHEMA surface once that it is in accordance with the expectation of two distinct molecular environments for the imidazole-carbamate nitrogens [36]. The peak centered at 401.2 eV is assigned to inner imidazole-ring nitrogen and, at 399.1 eV, the other peak includes the contribution of carbamate groups (NH(CO)O) and likely N of unreacted CDI imidazole groups [51]. Also

as expected, when the peptide was present the imidazole doublet almost disappears (Figure 7 B), since the peak corresponding to 401.2 eV critically decreases and the 399.1 eV peak is slightly dislocated to 399.9 eV (close to the 400 eV previously described by Ratner et al.) and becomes dominant, arising from the replacement of the imidazole ring structure for the amide bond through which the protein is linked to the pHEMA surface [36]. Together with the previous Nitrogen percentage results, and being in close conformity with the immobilization chemistry, these alterations in the N(1s) high-resolution spectra clearly show that the activation of the pHEMA surface and the subsequent immobilization of IgG on the activated surface were successful. As a result, the antibody of interest, a $F(ab')_2$ antihuman IgG-Fc specific fragment, could be immobilized using the range of CDI concentrations (0 to 30 mg/mL). In order to evaluate the surface morphologies of the pHEMA and CDI-activated protein-immobilized-pHEMA, SEM was performed. It is possible to observe, either at 200x and 500x magnification, that cross-linked pHEMA disks have a smooth homogeneous surface, pointing towards the low-fouling properties of pHEMA, of foremost importance when biomedical applications are concerned.

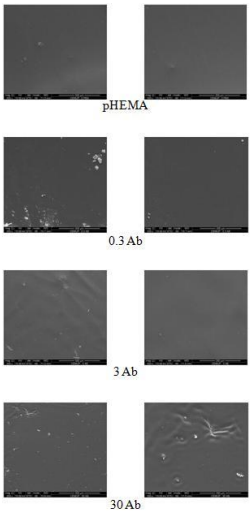

Figure 8- Scanning electron micrographs at two different magnifications (left images:200x; right image: 500x) of a pHEMA cross-linked gel, and $F(ab')_2$ antihuman IgG-Fc specific fragment (10 µg/mL)-immobilized pHEMA, with CDI concentration of 0.3, 3 and 30 mg/mL (0.3 Ab, 3 Ab and 30 Ab, respectively).

Although previous works have shown that surface modifications of pHEMA are illustrated by alterations on surface morphology visualized by SEM, in this case that was not observed [43]. On the referred works, different levels of C18 ligand were immobilized on pHEMA, comprising a different immobilization chemistry that could have lead to some reticulation which was not detected here. All the analyzed conditions (pHEMA and CDI-activated pHEMA with protein immobilized at 0.3, 3 and 30 mg/mL CDI concentrations) have shown no significant morphologic differences that could be visualized by SEM. Each and every one presented a smooth surface, with a few microscopic spots of sodium chloride (NaCl) crystals, identified by energy dispersive X-ray spectroscopy (EDS) analysis (data not shown). These observations can be explained by the use of Phosphate Buffered Saline (PBS) as protein solvent in which the disks were soaked before being dried out for SEM analysis. In subsequent experiments, the washing procedure was improved by soaking the samples three times in Milli-Q water after immobilization. This could help to avoid the PBS presence, which can also be deceptive within XPS analysis via creating, in some zones of the disks, a superficial crystal layer masking the signal of the investigated elements. Although struggled by BCA and ELISA, the detection of $F(ab')_2$ antihuman IgG-Fc specific fragment was not explicit, in BCA most likely given to the low antibody concentration present (significantly lower than the theoretical bottom sensitiveness of the method, 20 µg/mL) and in ELISA due to the high background perceived, probably originated from non-specific binding to pHEMA disks derived from the high Anti-rabbit IgG peroxidase dilution factor exercised (data not shown).

III.1.4 BINDING OF DELTA-1

Following the immobilization of the $F(ab')_2$ antihuman IgG-Fc specific fragment, Delta-1-extIgG, a chimeric form of Delta-1 with an Fc fragment of a human immunoglobulin, was bound to the functionalized polymeric surfaces (Figure 1). The rationale for binding the Notch ligand by its Fc region is to uniformly orient the protein, exposing the DSL region, which will permit the binding region to freely interact with the Notch receptor on the surface of the cell [27]. Although XPS analysis can indicate N presence and, thus, indirectly suggest the presence of proteins in a surface, it does not provide any clues about protein exposure and orientation (data not shown). Therefore, a "home-made" ELISA for Delta-1 was performed on ligand-Ab-surfaces previously prepared (Figure 9). Since Delta-1-extIgG is a chimeric protein, two different antibodies against different protein regions were tested: monoclonal anti-human Dll-1 antibody (against extracellular domain of Delta-1) and an anti-human IgG1, Fc fragment (against the Fc region of Delta-1-extIgG). The use of both antibodies would perceive if Delta-1 correct orientation was correctly achieved (if the ligand had not been bounded through its Fc tail, the later would be exposed and possibly detectable by an Anti-Fc antibody). Of notice is the fact that high background absorbance values were found on pHEMA samples, suggesting once more interferences on the low-fouling capacity of the prepared pHEMA. Even so and eliminating the background, the results at Figure 9 tend to be slightly higher for anti-Dll-1 antibody versus Anti-IgG1-Fc, suggesting the possible correct ligand orientation. Thus, aiming to quantify the bounded ligand with the correct orientation, along all range of CDI concentrations, other ELISA assay was performed (utilizing the Anti-Dll-1 monoclonal antibody).

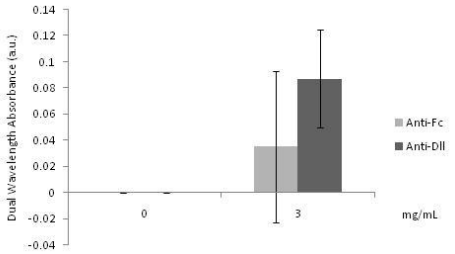

Figure 1- Comparison of orientation of immobilized Delta-1 on previously CDI-activated (3 mg/mL) and non-activated (CDI 0) pHEMA disks by ELISA using two different antibodies: Anti-human IgG1, Fc fragment (Anti-Fc) and anti-human Delta-1 (Anti-Dll).

However, and although the quantity of Delta-1 showed a tendency to increase along with the CDI concentration, a high background signal was obtained once more (data not shown). To counteract this drawback of ELISA test in pHEMA samples, alternative methods to quantify the amount of Delta-1 on the surface should be used in the future. An adequate alternative could be the use of radiolabeled-Delta-1 since protein radiolabeling is known as a high accurate, sensitive method to characterize protein adsorption [17,36,43].

III.2. ACTIVATION OF NOTCH SIGNALING BY DELTA-1-PHEMA SUBSTRATES

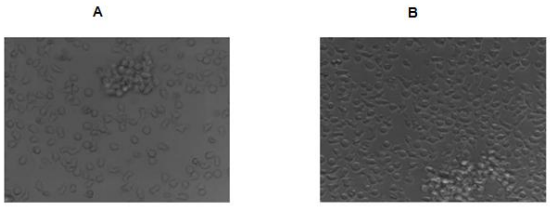

Figure 10- T-ALL-1-EGFP cell lines ($2x10^5$) morphology in the presence of adsorbed (A) and immobilized (B) Delta-1 at 96h of culture. The brightfield images were obtained at a magnification of 100x.

The proof of concept of the biomaterials developed is to evaluate the biofunctionality of immobilized Delta1, i.e. to evaluate its potential to activate Notch signaling pathway. To study Notch signaling activation, a T-cell lymphoblastic leukemia (T-ALL) cell line encoding the enhanced green fluorescent protein (EGFP) reporter gene under the control of the Notch3 promoter (TALL-1-rbs-EGFP) was used, and EGFP intensity by Delta-1 stimulation was monitored by flow cytometry. Subsequent to optimization steps, it was achieved that the seeding density of $2x10^5$ cells/mL and the activation period of 96h were the optimal conditions for the stimulation of TALL-1-rbs-EGFP cells with Delta-1 (data not shown). Furthermore, cell morphology does not appear to be affected by Notch receptor stimulation (Figure 10). As expected, some cell clusters were observed as well as the characteristic pleomorphic shape, with some cells with elongated configuration and cytoplasmatic tails, of T-ALL cells [52]. Despite not having been counted, the apparently higher number of cells within the immobilized-ligand condition may possibly point towards an effective Notch signaling-induced proliferative effect on T-ALL cells. Considering Notch receptor activation by Delta-1-TCPS samples with and without Ab (Figure 11), it can be noticed the positive effect of Ab presence on receptor activation. This proves evidence that ligand orientation, which is not controlled when the ligand is adsorbed directly to TCPS but is achieved when the ligand is bounded to Ab through its Fc domain, is of foremost importance for Notch signaling activation [27]. In what respects to Notch activation by immobilized Delta-1 on pHEMA disks, it is clear in that all the surfaces were able to activate the Notch receptor on the T-ALL cells (Figure 11)

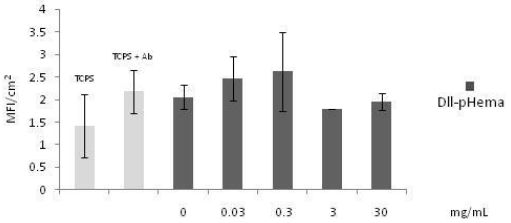

Figure 11- Triggering of Notch signaling in T-ALL-1-rbs-EGFP cells, $2x10^5$ cells/mL, after 96 hours of stimulation with Delta-1 ligand (10 µg/mL). The cells were cultured onto Ab-pHEMA disks with five different CDI concentration (i.e.: five different Ab immobilization levels): 0; 0.03; 0.3; 3 and 30 mg/mL ("Dll-pHEMA" series). The median fluorescent intensity (MFI) per area was also assessed for cells plated onto TCPS wells and to TCPS wells with adsorbed Ab (TCPS+Ab), both with the ligand.

Although small differences were observed in the frequency of cells expressing EGFP (<1%) between the conditions evaluated, a slightly higher percentage was observed for surfaces activated with low to intermediate CDI concentrations (data not shown). This observation is confirmed by the higher signaling activation levels in Figure 11. In previous results, it is described that Delta-1 concentration on the surfaces seemed to increase with the amount of immobilized Ab (due to the increase on CDI concentration) (XPS analysis). Nevertheless, the same trend was not observed concerning the receptor activation. Interestingly, in agreement with previous studies using model surfaces (self-assembled monolayers), higher Notch activation levels were achieved using low ligand concentrations [17]. Using SAMs with immobilized Ab, 0.03 mg/mL of CDI was found to be the adequate concentration to better expose the ligand and induce higher activation levels. In this case, although without significant differences, a similar trend was observed, with 0.3 mg/mL of CDI being the activator concentration responsible for the highest activation levels. This may be due to intermediate ligand concentrations (thus not fully covering the activated surface) turn the ligand more accessible to be recognized in terms of available space for the cell to bind. Also, ligand orientation (i.e. better exposition of its DSL region, the portion of the ligand that activate the receptor) by Ab immobilization can improve ligand binding to TALL-1 cell Notch receptors. In addition, the lower differences observed between conditions, when compared to what

was obtained on SAMs, may be related to the fact that different methods to measure ligand activity were exploited [17]. Herein, EGFP (protein) expression was quantified, while in previous studies (Gonçalves et al.) it was assessed the expression of Notch target gene Hes-1 by quantitative PCR, which may comprise higher sensitivity. Furthermore, the high ligand adsorption levels noticed on pHEMA may also have contributed for observing lower differences of Notch activation among the tested conditions. Alternative approaches could be used to quantify Notch pathway activation: i) the assessment of Notch target genes (e.g. the HES-1 notch regulated gene family) transcription in response to the bound ligand; ii) the detection, by Western Blot, of Notch3 signaling intermediates (e.g. intracellular domain of Notch3 receptor) throughout the signaling pathway.

IV. Conclusion and Future Trends

The work developed in this thesis fulfilled the proposed objectives and contributes for the ambitious aim of converting Notch as a therapeutic target using biomaterials specifically designed. From the work previously developed using model surfaces, the knowledge was transposed to a biocompatible polymer, being an important step to achieve a range of Notch levels by immobilized ligands with controlled orientation. Therefore, the implemented strategy is the first step on novel biomaterials that may serve as a platform to take a deeper look into molecular aspects of Notch signaling pathway. In particular, due to the potential of Notch to increase HSC numbers, ex vivo HSC expansion emerges as the more imminent application of the present biomaterial [23,25,52]. The gradient density of immobilized ligands predicted by this strategy may bring new insights in the understanding of Notch ligands dose dependence within the HSC ex vivo expansion, and may represent a key feature in the development of more effective systems for the expansion of HSC for clinical purposes [21]. Still, the potential of this system is too prominent to "simply" confine it to the HSC expansion field. It is achieved that, in cancer, the Notch pathway can be either oncogenic or tumor suppressive depending on the tissue and organ site in which it is expressed [16,53]. The present approach may serve as a platform to study the influence of Notch ligand densities among diverse cancer systems, one of the possible causes of the antagonistic effects of Notch (similarly to what occurs in the hematopoietic system), which was never addressed, to our best knowledge [20,21]. In fact, Notch signaling has a soaring role in a myriad of diseases. This cascade has recently been shown to be also associated with autoimmune and cardiac diseases, and suggested to play a part in the neurodegeneration observed in Alzheimer's disease and within the pathogenesis of skin diseases as psoriasis [54-57]. These evidences, together with the significance of having the ligand immobilized and correctly exposed at different densities, and with the advantages of biocompatible synthetic polymers, render the therapeutic potential of the developed substrates inestimable. Although preliminary, the outcome of this thesis though biomaterials science is a step forward on Notch pathway control that may have drastic implications in biological and medical sciences.

V. References

1. Covas, D. T. & Zago, M. A. Células-tronco - A nova fronteira da medicina. (Etheneu, 2006).
2. Weissman, I. L. & Shizuru, J. A. The origins of the identification and isolation of hematopoietic stem cells, and their capability to induce donor-specific transplantation tolerance and treat autoimmune diseases. *Blood* **112**, 3543-3553 (2008).
3. Cabral, J. M. S. Ex vivo expansion of hematopoietic stem cells in bioreactors. Biotechnology Letters 23, 741-751 (2001).
4. de Lima, M. *et al.* Transplantation of ex vivo expanded cord blood cells using the copper chelator tetraethylenepentamine: a phase I/II clinical trial. *Bone Marrow Transplant* **41**, 771-778 (2008).
5. Stanevsky, A., Shimoni, A., Yerushalmi, R. & Nagler, A. Cord Blood Stem Cells for Hematopoietic Transplantation. *Stem Cell Reviews and Reports*, 1-9, doi:10.1007 (2010).
6. Zhang, C. C., Kaba, M., Iizuka, S., Huynh, H. & Lodish, H. F. Angiopoietin-like 5 and IGFBP2 stimulate ex vivo expansion of human cord blood hematopoietic stem cells as assayed by NOD/SCID transplantation. *Blood* **111**, 3415-3423, doi:10.1182/blood-2007-11-122119 (2008).
7. Choi, Y.-S., Noh, S.-E., Lim, S.-M. & Kim, D.-i. Optimization of ex vivo hematopoietic stem cell expansion in intermittent dynamic cultures. *Biotechnology Letters*, 1-7, doi:10.1007/s10529-010-0355-0 (2010).
8. Jing, D. *et al.* Hematopoietic stem cells in co-culture with mesenchymal stromal cells - modeling the niche compartments in vitro. *Haematologica* **95**, 542-550, doi:10.3324/haematol.2009.010736 (2010).
9. HAYASHI *et al. The Effects of X-Irradiation on Ex Vivo Expansion of Cryopreserved Human Hematopoietic Stem/Progenitor Cells*. Vol. 51 (Japan Radiation Research Society, 2010).
10. Renström, J., Kröger, M., Peschel, C. & Oostendorp, R. A. J. How the niche regulates hematopoietic stem cells. Chemico-Biological Interactions 184, 7-15, doi:DOI: 10.1016/j.cbi.2009.11.012 (2010).
11. Mishima, S. *et al.* Effective ex vivo expansion of hematopoietic stem cells using osteoblast-differentiated mesenchymal stem cells is CXCL12 dependent. *European Journal of Haematology* **84**, 538-546, doi:10.1111 (2010).
12. Nishino, T. *et al.* Ex vivo expansion of human hematopoietic stem cells by a small-molecule agonist of c-MPL. *Experimental Hematology* **37**, 1364-1377.e1364, doi:DOI: 10.1016/j.exphem.2009.09.001 (2009).
13. Lee, J. & Kotov, N. A. Notch Ligand Presenting Acellular 3D Microenvironments for ex vivo Human Hematopoietic Stem-Cell Culture made by Layer-By-Layer Assembly. *Small* **5**, 1008-1013, doi:10.1002/smll.200801242 (2009).
14. da Silva, C. L. *et al.* A human stromal-based serum-free culture system supports the ex vivo expansion/maintenance of bone marrow and cord blood hematopoietic stem/progenitor cells. *Experimental Hematology* **33**, 828-835, doi:DOI: 10.1016/j.exphem.2005.03.017 (2005).
15. Kanai, M. *et al.* Stromal cell-dependent ex vivo expansion of human cord blood progenitors and augmentation of transplantable stem cell activity. *Bone Marrow Transplantation* **26**, 837-844 (2000).
16. Yin, L., Velazquez, O. C. & Liu, Z.-J. Notch signaling: Emerging molecular targets for cancer therapy. *Biochemical Pharmacology* **80**, 690-701, doi:DOI: 10.1016/j.bcp.2010.03.026 (2010).
17. Gonçalves, R. M., Martins, M. C. L., Almeida-Porada, G. & Barbosa, M. A. Induction of notch signaling by immobilization of jagged-1 on self-assembled monolayers. *Biomaterials* **30**, 6879-6887, doi:DOI: 10.1016/j.biomaterials.2009.09.010 (2009).

18. Rose, S. L., Kunnimalaiyaan, M., Drenzek, J. & Seiler, N. Notch 1 signaling is active in ovarian cancer. *Gynecologic Oncology* **117**, 130-133, doi:DOI: 10.1016 (2010).
19. Oswald, F. *et al.* p300 Acts as a Transcriptional Coactivator for Mammalian Notch-1. *Mol. Cell. Biol.* **21**, 7761-7774, doi:10.1128/mcb.21.22.7761-7774.2001 (2001).
20. Bernstein, I. D. et al. Density of the Notch ligand Delta1 determines generation of B and T cell precursors from hematopoietic stem cells. *The Journal of Experimental Medicine* **201**, 1361-1366, doi:10.1084/jem.20042450 (2005).
21. Bernstein, I. D. et al. Dose-dependent effects of the Notch ligand Delta1 on ex vivo differentiation and in vivo marrow repopulating ability of cord blood cells. *Blood* **106**, 2693-2699, doi:10.1182/blood-2005-03-1131 (2005).
22. Leong, K. G. & Karsan, A. Recent insights into the role of Notch signaling in tumorigenesis. *Blood* **107**, 2223-2233, doi:10.1182/blood-2005-08-3329 (2006).
23. Zhou, K. *et al.* Wnt and Notch signaling pathways selectively regulating hematopoiesis. *Annals of Hematology* **89**, 749-757, doi:10.1007/s00277-010-0923-3 (2010).
24. Indraccolo, S. *et al.* Cross-talk between Tumor and Endothelial Cells Involving the Notch3-Dll4 Interaction Marks Escape from Tumor Dormancy. *Cancer Research* **69**, 1314-1323, doi:10.1158/0008-5472.can-08-2791 (2009).
25. Delaney, C. *et al.* Notch-mediated expansion of human cord blood progenitor cells capable of rapid myeloid reconstitution. *Nat Med* **16**, 232-236, doi:http://www.nature.com/nm/journal/v16/n2/suppinfo/nm.2080_S1.html (2010).
26. Beckstead, B. L., Santosa, D. M. & Giachelli, C. M. Mimicking cell–cell interactions at the biomaterial–cell interface for control of stem cell differentiation. *Journal of Biomedical Materials Research Part A* **79A**, 94-103, doi:10.1002/jbm.a.30760 (2006).
27. Beckstead, B. L. *et al.* Methods to promote Notch signaling at the biomaterial interface and evaluation in a rafted organ culture model. *Journal of Biomedical Materials Research Part A* **91A**, 436-446, doi:10.1002/jbm.a.32214 (2009).
28. Gonçalves, R et al.. Bioactivity of immobilized EGF on self-assembled monolayers: Optimization of the immobilization process. *Journal of Biomedical Materials Research Part A* **94A**, 576-585, doi:10.1002/jbm.a.32723 (2010).
29. Taqvi, S., Dixit, L. & Roy, K. Biomaterial-based notch signaling for the differentiation of hematopoietic stem cells into T cells. *Journal of Biomedical Materials Research Part A* **79A**, 689-697, doi:10.1002/jbm.a.30916 (2006).
30. Varnum-Finney, B. *et al.* Immobilization of Notch ligand, Delta-1, is required for induction of notch signaling. *J Cell Sci* **113**, 4313-4318 (2000).
31. Martins, M. C. L. *et al.* Molecularly designed surfaces for blood deheparinization using an immobilized heparin-binding peptide. *Journal of Biomedical Materials Research Part A* **88A**, 162-173, doi:10.1002/jbm.a.31849 (2009).
32. Freitas, S. C., Barbosa, M. A. & Martins, M. C. L. The effect of immobilization of thrombin inhibitors onto self-assembled monolayers on the adsorption and activity of thrombin. *Biomaterials* **31**, 3772-3780, doi:10.1016/j.biomaterials.2010.01.097 (2010).
33. Puleo, D. A. & Bizios, R. *Biological Interactions on Materials Surfaces*. (2009).
34. Pal, K., Banthia, A. K. & Majumdar, D. K. Polymeric hydrogels: Characterization and biomedical applications. *Designed Monomers and Polymers* **12**, 197-220 (2009).
35. Jagur-Grodzinski, J. Polymeric gels and hydrogels for biomedical and pharmaceutical applications. *Polymers for Advanced Technologies* **21**, 27-47, doi:10.1002 (2010).
36. Martin, S. M. *et al.* Characterization and analysis of osteopontin-immobilized poly(2-hydroxyethyl methacrylate) surfaces. *Journal of Biomedical Materials Research Part A* **67A**, 334-343, doi:10.1002/jbm.a.10060 (2003).
37. Ratner, B. D., Hoffman, A. S., Schoen, F. J. & Lemons, J. E. *Biomaterials Science: An Introduction to Materials in Medicine*. (Elsevier, 2004).
38. Hong, K., Jeon, Y.-S., Chung, D. & Kim, J.-H. Drug release characteristics of modified PHEMA hydrogel containing thermo-responsive pluronic copolymer. *Macromolecular Research* **18**, 204-207, doi:10.1007 (2010).
39. Tang, Q., Yu, J.-R., Chen, L., Zhu, J. & Hu, Z.-M. Preparation and properties of morphology controlled poly(2-hydroxyethyl methacrylate)/poly(N-vinyl pyrrolidone) double networks for biomedical use. *Current Applied Physics* **10**, 766-770, doi:DOI: 10.1016/j.cap.2009.09.012 (2010).
40. Martins, M. C. L., Wang, D., Ji, J., Feng, L. & Barbosa, M. A. Albumin and fibrinogen adsorption on PU-PHEMA surfaces. *Biomaterials* **24**, 2067-2076, doi:Doi: 10.1016 (2003).
41. Sousa, S., Moradas-Ferreira, P. & Barbosa, M. TiO₂ type influences fibronectin adsorption. *Journal of Materials Science: Materials in Medicine* **16**, 1173-1178, doi:10.1007/s10856-005 (2005).
42. Heck, D. E., Bisaccia, E., Armus, S. & Laskin, J. D. Production of hydrogen peroxide by cutaneous T-cell lymphoma following photopheresis with psoralens and ultraviolet light. *Cancer Chemotherapy and Pharmacology* **28**, 344-350, doi:10.1007/bf00685687 (1991).
43. Gonçalves, I. C., Martins, M. C. L., Barbosa, M. A. & Ratner, B. D. Protein adsorption and clotting time of pHEMA hydrogels modified with C18 ligands to adsorb albumin selectively and reversibly. *Biomaterials* **30**, 5541-5551, doi:DOI: 10.1016/j.biomaterials.2009.06.025 (2009).
44. Perova, T., Vij, J. & Xu, H. Fourier transform infrared study of poly (2-hydroxyethyl methacrylate) PHEMA. *Colloid & Polymer Science* **275**, 323-332, doi:10.1007 (1997).
45. Taylor, C. E., Garvey, S. D. & Pemberton, J. E. Carbon Contamination at Silver Surfaces: Surface Preparation Procedures Evaluated by Raman Spectroscopy and X-ray Photoelectron Spectroscopy. *Analytical Chemistry* **68**, 2401-2408, doi:10.1021/ac950753h (1996).
46. Lee, H. J., Nedelkov, D. & Corn, R. M. Surface Plasmon Resonance Imaging Measurements of Antibody Arrays for the Multiplexed Detection of Low Molecular Weight Protein Biomarkers. *Analytical Chemistry* **78**, 6504-6510, doi:10.1021/ac060881d (2006).
47. Socrates, G. *Infrared and Raman Characteristic Group Frequencies - Tables and charts*. third edition edn, (Wiley, 2000).
48. de Figueiredo, R. M., Fröhlich, R. & Christmann, M. N,N'-Carbonyldiimidazole-Mediated Cyclization of Amino Alcohols to Substituted Azetidines and Other N-Heterocycles. *The Journal of Organic Chemistry* **71**, 4147-4154, doi:10.1021/jo060130b (2006).
49. Goddard, J. & Erickson, D. Bioconjugation techniques for microfluidic biosensors. *Analytical and Bioanalytical Chemistry* **394**, 469-479, doi:10.1007/s00216-009-2731-y (2009).
50. Hermanson, G. T. *Bioconjugate Techniques*. (Elsevier, 2008).
51. Boufi, S. et al. Grafting of Porphyrins on Cellulose Nanometric Films. *Langmuir* **24**, 7309-7315, doi:10.1021 (2008).
52. Jonathan, M. W. & Laura, M. C. Notch signaling and the bone marrow hematopoietic stem cell niche. *Bone* **46**, 281-285 (2010).
53. Lai, E. C. Notch signaling: control of cell communication and cell fate. *Development* **131**, 965-973, doi:10.1242/dev.01074 (2004).
54. de la Pompa, J. Notch Signaling in Cardiac Development and Disease. *Pediatric Cardiology* **30**, 643-650, doi:10.1007/s00246-008-9368-z (2009).
55. Ma, D., Zhu, Y., Ji, C. & Hou, M. Targeting the Notch signaling pathway in autoimmune diseases. *Expert Opinion on Therapeutic Targets* **14**, 553-565 (2010).
56. Okuyama, R., Tagami, H. & Aiba, S. Notch signaling: Its role in epidermal homeostasis and in the pathogenesis of skin diseases. *Journal of Dermatological Science* **49**, 187-194 (2008).
57. Woo, H. et al. Alzheimer's disease and Notch signaling. *Biochemical and Biophysical Research Communications* **390**, 1093-1097, doi:DOI: 10.1016/j.bbrc.2009.10.093 (2009).